Skeletal Editing by Tip-Induced Chemistry

Citation for the original published paper (version of record):
Mishra, S., Malave, V., Svensson, R. et al (2025). Skeletal Editing by Tip-Induced Chemistry. Journal of the American Chemical Society, 147(48): 44055-44059.
http://dx.doi.org/10.1021/jacs.5c16196

JACS
JOURNAL OF THE AMERICAN CHEMICAL SOCIETY

pubs.acs.org/JACS
Communication

Skeletal Editing by Tip-Induced Chemistry

Shantanu Mishra,* Valentina Malave,# Rasmus Svensson,# Henrik Grönbeck, Florian Albrecht, Diego Peña,* and Leo Gross*

Cite This: J. Am. Chem. Soc. 2025, 147, 44055−44059
Read Online
ACCESS | Metrics & More | Article Recommendations | Supporting Information

ABSTRACT: Skeletal editing of cyclic molecules has garnered considerable attention in the context of drug discovery and green chemistry with notable examples in solution-phase synthesis. Here, we extend the scope of skeletal editing to the single-molecule scale. We demonstrate tip-induced oxygen deletion and ring contraction of an oxygen-containing seven-membered ring on bilayer NaCl films to generate molecules containing the perylene skeleton. The products were identified and characterized at the atomic scale by atomic force microscopy and scanning tunneling microscopy. Insights into the reaction mechanisms were obtained by density functional theory calculations. Our work expands the toolbox of tip-induced chemistry for single-molecule synthesis.

Skeletal editing[1] refers to the modification of the cyclic skeleton of an organic molecule by inserting, deleting, or swapping individual atoms at precise locations at late stages of a synthetic sequence. The process is schematically depicted in Scheme 1, where it is contrasted with peripheral editing. Skeletal editing is poised to be of great importance in medicinal chemistry,[2,3] where precise edits to the molecular skeleton without the design of new synthetic routes from scratch could dramatically speed up drug discovery. Skeletal editing has also been employed to modify polymer backbones,[4] which may open avenues for upcycling of plastics. The current repertoire of skeletal editing in solution-phase chemistry includes (a) deletion[5−7] and insertion[8−10] of C, N, and O atoms; (b) swapping[11−13] of ^{12}C with ^{13}C, N, and O; and (c) ring contraction[14] and expansion.[15] In this context, tip-induced chemistry,[16,17] wherein voltage pulses applied by a scanning probe tip are used to induce chemical reactions of molecular species adsorbed on surfaces, holds distinct advantages. Atomic-scale structural and electronic characterizations of molecular species can be performed by scanning tunneling microscopy (STM) and atomic force microscopy (AFM). Furthermore, the solvent-free, cryogenic, and ultrahigh-vacuum conditions facilitate generation (sometimes with high selectivity[18]), stabilization, and characterization of reactive intermediates and products, which can yield mechanistic insights into chemical reactions. Tip-induced chemistry has been successfully employed to generate molecules by peripheral editing, such as through dissociation of C−Cl,[18,19] C−Br,[20,21] C−I,[22] C−C,[23,24] C−H,[25,26] C−O,[27] N−H,[28] and N−N[29] bonds, attachment of foreign molecules,[30] and skeletal rearrangement.[31,32] Here, we demonstrate tip-induced skeletal editing (Scheme 1). From dinaphtho[1,8-*bc*:1′,8′-*ef*]oxepine (**DNO**), we generated different molecules with the perylene skeleton by oxygen deletion, and ring contraction and oxygen migration.

DNO was synthesized by solution-phase chemistry (Schemes S1−S5 and Figures S1−S7) and deposited on a single-crystal Cu(111) surface partially covered by bilayer NaCl films (Figure S8). Figure 1a shows an STM image of the surface, revealing isolated **DNO** molecules, along with coadsorbed carbon monoxide (CO) molecules and a minority of third-layer NaCl islands. Nearly all **DNO** molecules (66 out of 67 imaged **DNO** molecules) on NaCl adopted an adsorption conformation wherein the oxygen atom points toward the surface (denoted O-down). Figures 1b−d show STM and AFM images of an O-down **DNO** molecule. In AFM imaging at large tip heights (Figure 1c), only two benzenoid rings of the molecule are visible, and in imaging at small tip heights, all four benzenoid rings become visible (Figure 1d). Related to the adsorption geometry, the oxygen atom is not visible. The conspicuous streaks in the STM and AFM images likely result from conformational switching of the molecule under the influence of the tip, related to the relative tilting of the benzenoid rings. Rarely, we found **DNO** molecules on NaCl wherein the oxygen atom points away from the surface (O-up, Figures 1e−g). In this case, the oxygen atom, being the atomic species closest to the tip, appears bright in AFM imaging (that is, with an increased frequency shift Δf). Density functional theory (DFT) calculations of **DNO** on NaCl/Cu(111) predicted the O-down conformation to be ∼0.1 eV more stable than the O-up conformation, in line with the experimentally observed predominance of the O-down species. Figure S9 shows further measurements on **DNO**.

Voltage pulses ranging between 4.9 and 5.1 V were applied to individual **DNO** molecules by the tip of the STM/AFM system to trigger intramolecular chemical reactions (Methods and Figure S10). From 99 voltage pulses applied to 28 **DNO** molecules, we observed 21 molecules that underwent a reaction on the surface, resulting in 6 unique species. In

Received: September 15, 2025
Revised: November 7, 2025
Accepted: November 12, 2025
Published: November 20, 2025

https://doi.org/10.1021/jacs.5c16196
J. Am. Chem. Soc. 2025, 147, 44055−44059

Scheme 1. (a) Illustration of Skeletal and Peripheral Editing;[a] (b) Scheme Showing the Generation of the Two Majority Products by Tip-Induced Skeletal Editing of DNO

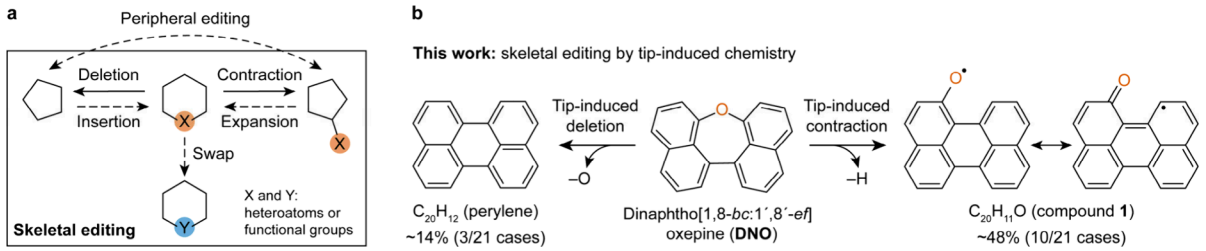

[a]The solid arrows denote the skeletal editing reactions observed in this work.

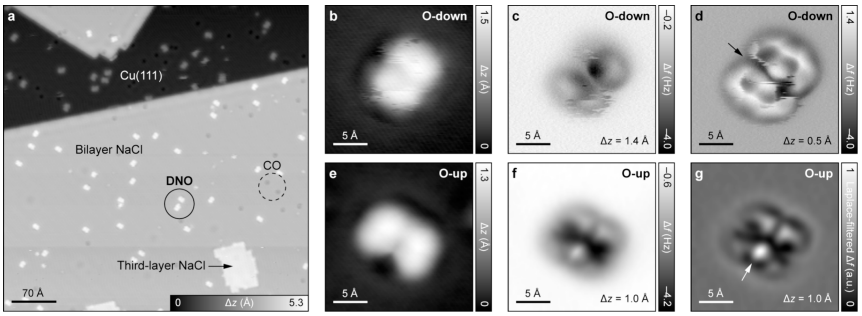

Figure 1. Characterization of **DNO** on NaCl/Cu(111). (a) STM overview image of the sample. (b–d) STM (b) and AFM (c, d) images of an O-down DNO molecule. (e–g) STM (e), AFM (f), and the corresponding Laplace-filtered AFM (g) images of an O-up **DNO** molecule. The arrows in (d, g) indicate the location of the oxygen atom. Scanning parameters for STM images: V = 0.2 V, I = 0.5 pA. Open feedback parameters for AFM images: V = 0.2 V, I = 0.5 pA on NaCl. Δz denotes the tip-height offset, with positive (negative) values indicating tip retraction (approach) from the set-point conditions.

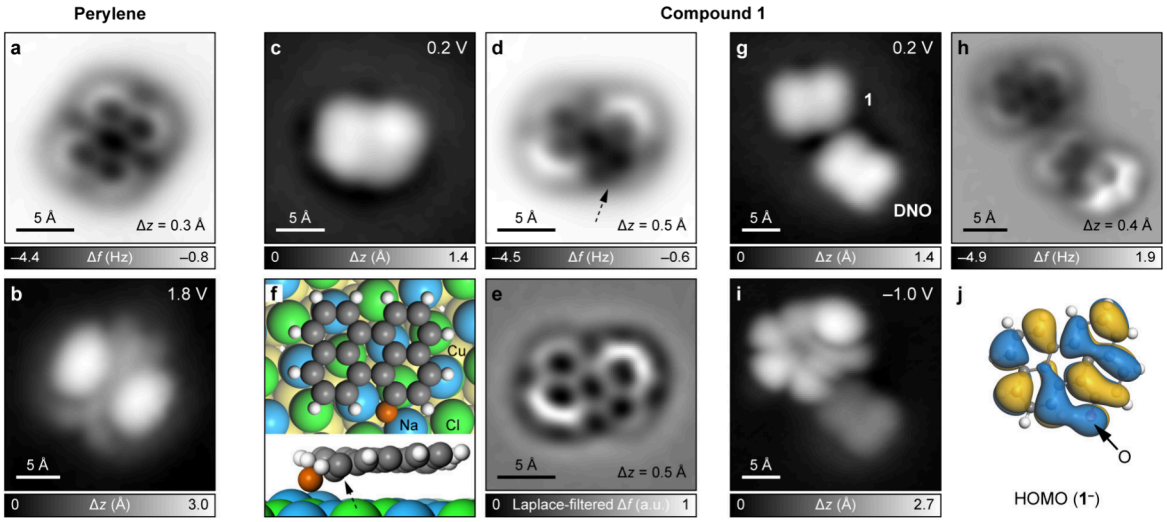

Figure 2. Structural and electronic characterizations of perylene and compound **1**. (a) AFM image of perylene. (b) STM image of perylene showing its LUMO density. (c–e) STM (c), AFM (d), and corresponding Laplace-filtered AFM (e) images of $\mathbf{1}^-$. (f) Top and side views of the DFT-calculated adsorption geometry of $\mathbf{1}^-$ on bilayer NaCl/Cu(111). The oxygen atom adsorbs bridging two Na^+ ions, which show an outward relaxation of ~0.5 Å. The arrows in (d, f) indicate the six-membered ring bonded to the oxygen atom. C, H, and O atoms are colored gray, white, and orange, respectively. (g, h) STM (g) and AFM (h) images of $\mathbf{1}^-$ adsorbed next to a **DNO** molecule. (i) Corresponding STM image showing the HOMO density of $\mathbf{1}^-$. (j) DFT-calculated HOMO of $\mathbf{1}^-$ (isosurface: 0.01 $a_0^{-3/2}$, a_0 denotes the Bohr radius). Scanning parameters for STM images: I = 0.15 pA (b), I = 0.5 pA (c), and I = 0.3 pA (g, i). Open feedback parameters for AFM images: V = 0.2 V, I = 0.5 pA on NaCl.

unsuccessful cases, **DNO** molecules were either displaced on NaCl and remained intact, or were not located, presumably being picked up by the tip or displaced from NaCl onto Cu(111). Out of the 21 reacted molecules, the majority (16/21) corresponded to molecules with the perylene skeleton (constituting 4 species), namely, perylene (3/21), 1-perylenoxy radical (compound **1**; 10/21), perylenyl radical (compound **2**; 2/21), and didehydroperylene (compound **3**; 1/21). In cases where the oxygen atom was removed from **DNO** (as in perylene, **2**, and **3**), the oxygen atom was not found on the surface, likely because of its desorption to the gas phase or diffusion on NaCl followed by adsorption on Cu(111). Here, we focus on the characterization of perylene and **1**, the major products of atom deletion and ring

https://doi.org/10.1021/jacs.5c16196
J. Am. Chem. Soc. 2025, 147, 44055–44059

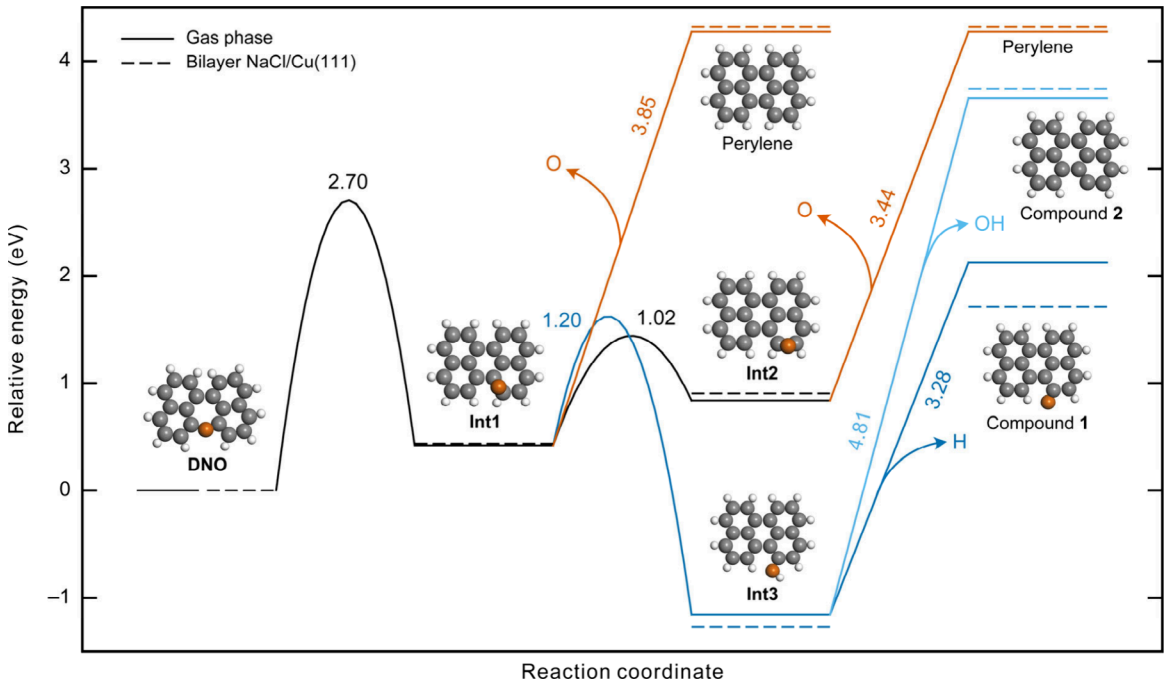

Figure 3. Ab initio potential energy landscape in the gas phase (solid lines) and on bilayer NaCl/Cu(111) (dashed lines) for skeletal editing of DNO. The optimized gas-phase geometries of DNO, intermediates, and products are also shown. The numbers adjacent to the curves denote absolute gas-phase activation energies in eV. Note that for the reactions **Int1** and **Int2** → perylene and **Int3** → compounds **1** and **2**, energy differences coincide with activation energies. For on-surface calculations, gas-phase barrier heights are used, and the dissociated O, H, and OH species are assumed to desorb.

contraction, respectively. The characterizations of **2** and **3** are reported in Figure S11, and data on the remaining two species (5/21 cases) are shown in Figure S12.

Figure 2a shows an AFM image of perylene generated by the tip-induced removal of an oxygen atom from **DNO**. STM imaging at bias voltage V = 1.8 V (Figure 2b) revealed the lowest unoccupied molecular orbital (LUMO) density of perylene, in agreement with calculations (Figure S13). We next focused on the characterization of **1**, which maintains an oxygen atom attached to the perylene skeleton (Scheme 1). At the outset, we note that **1** is found in an anionic charge state on the surface (denoted as $\mathbf{1}^-$). This is experimentally inferred from the scattering of the NaCl/Cu(111) interface state by the molecule (Figure S14) and supported by Bader charge analysis of the molecule adsorbed on bilayer NaCl/Cu(111), yielding a transfer of 0.81 electrons from the surface to **1**. In contrast to charge-neutral **1** (denoted $\mathbf{1}^0$) being an open-shell species, $\mathbf{1}^-$ is closed-shell (Figure S15). The optimized C−O bond length of $\mathbf{1}^-$ on bilayer NaCl/Cu(111) is calculated to be 1.29 Å. To contextualize this value in terms of the single- or double-bond character of the C−O bond, we carried out gas-phase calculations (Table S1) of cyclohexanone and phenol, which contain C(sp^2)−O double and single bonds, respectively. From these calculations, we obtained C−O bond lengths of 1.23 Å (cyclohexanone) and 1.38 Å (phenol). The comparison of the C−O bond lengths thus indicates that $\mathbf{1}^-$ is best described as a resonance hybrid of structures containing C−O single and double bonds (Scheme 1). Figures 2c−e show the STM and AFM images of $\mathbf{1}^-$. In AFM imaging of $\mathbf{1}^-$ (Figures 2d,e), the benzenoid ring bonded to an oxygen atom (highlighted by the arrow in Figure 2d) appears notably dark, whereas two peripheral benzenoid rings that lie diagonally opposite each other appear bright. This observation agrees with the DFT calculation of $\mathbf{1}^-$ on bilayer NaCl/Cu(111) (Figure 2f), which shows a nonplanar adsorption conformation of $\mathbf{1}^-$ with the oxygen atom pointing toward the surface and an upward tilt of the two peripheral benzenoid rings. Figures 2g,h show the STM and AFM images of $\mathbf{1}^-$ adsorbed next to a **DNO** molecule that rendered $\mathbf{1}^-$ stable for imaging at elevated voltages. We could therefore measure the highest occupied molecular orbital (HOMO) density of $\mathbf{1}^-$ at −1.0 V (Figure 2i), which exhibited good agreement with the calculated HOMO of $\mathbf{1}^-$ (Figure 2j).

Insights into the mechanisms of skeletal editing reactions were obtained by DFT calculations of the reaction landscape. Figure 3 summarizes the results and highlights the relevant reaction paths and energy barriers involved in the generation of perylene, **1**, and **2**. Given the weak molecule−surface interactions on NaCl, we focus on elucidating the reaction mechanisms in the gas phase (solid lines in Figure 3). Starting from **DNO**, the first step involves the formation of a C−C bond resulting in a central six-membered ring, along with migration of the oxygen atom to a neighboring C−C bridge site (intermediate **Int1**, activation energy $\Delta E^{\ddagger}$ = 2.70 eV). Three reaction paths are possible after the first step. First, the oxygen atom in **Int1** can be eliminated ($\Delta E^{\ddagger}$ = 3.85 eV), leading to the generation of perylene. Second, the oxygen atom in **Int1** can migrate to the next C−C bridge site ($\Delta E^{\ddagger}$ = 1.02 eV), leading to intermediate **Int2**, from where the oxygen atom can once again be eliminated ($\Delta E^{\ddagger}$ = 3.44 eV) to generate perylene. Third, a rearrangement reaction can occur, resulting in the formation of intermediate **Int3**. The reaction is exothermic and associated with $\Delta E^{\ddagger}$ = 1.20 eV. From **Int3**, either the hydroxy group can be removed to generate **2**, which requires a large $\Delta E^{\ddagger}$ of 4.81 eV, or the hydrogen atom can be removed from the hydroxy group to generate **1** ($\Delta E^{\ddagger}$ = 3.28

https://doi.org/10.1021/jacs.5c16196
J. Am. Chem. Soc. 2025, 147, 44055−44059

eV). We also calculated the potential energy landscape on bilayer NaCl/Cu(111) (dashed lines in Figure 3), where the relative energies of all intermediates and products are similar to those in the gas phase, apart from **1**, which is stabilized on the surface (Figure 2f). We note that intermediates **Int1**−**Int3** were not observed in the experiments. The gas-phase calculations in Figure 3 were performed assuming a neutral charge state of the reactant, intermediates, and products. We also performed gas-phase calculations assuming a global anionic state, which is a possibility given the large positive applied voltage pulses that could cause transient charging of the species. As shown in Figure S16, the reaction mechanisms in the anionic state are similar, but there is a notable lowering of all activation barriers compared to the neutral case. The importance of using the insulating NaCl surface to reduce molecule−surface interactions and facilitate skeletal editing is emphasized by the fact that we were unable to perform skeletal editing on Cu(111), where chemisorption of intermediates or competing reactions were observed instead (Figure S17).

In conclusion, we demonstrate skeletal editing via tip-induced chemistry. Voltage pulses applied by a scanning probe tip to dinaphtho[1,8-*bc*:1′,8′-*ef*]oxepine molecules adsorbed on NaCl resulted in two distinct skeletal editing reactions: atom deletion and ring contraction. The former predominantly led to the generation of perylene, whereas the latter led to the generation of 1-perylenoxy radical. Experimental characterization of the products was performed by STM and AFM, and a detailed mechanistic understanding of the intramolecular reactions was obtained from DFT calculations. Future directions could involve exploring how heteroatoms of the same group (such as sulfur) affect the reaction landscape and yields, and performing the challenging atom insertion and swap edits. Obtaining selectivity of the different skeletal editing reactions by tip-induced chemistry would be another goal. Tip-induced skeletal editing may be used for precise local modification of heteroatom-containing carbon nanostructures to imprint electronic[33−36] and magnetic[37] functionalities.

■ ASSOCIATED CONTENT

Supporting Information

The Supporting Information is available free of charge at https://pubs.acs.org/doi/10.1021/jacs.5c16196.

Experimental and theoretical methods, solution synthesis of **DNO**, ^{1}H and ^{13}C NMR spectra, mass spectroscopy data, STM and AFM data, and additional calculations (PDF)

■ AUTHOR INFORMATION

Corresponding Authors

Shantanu Mishra − *Department of Physics, Chalmers University of Technology, 412 96 Göteborg, Sweden; IBM Research Europe − Zurich, 8803 Rüschlikon, Switzerland;* orcid.org/0000-0002-2900-4203; Email: shantanu.mishra@chalmers.se

Diego Peña − *Center for Research in Biological Chemistry and Molecular Materials, and Department of Organic Chemistry, University of Santiago de Compostela, 15782 Santiago de Compostela, Spain; Oportunius, Galician Innovation Agency, 15702 Santiago de Compostela, Spain;* orcid.org/0000-0003-3814-589X; Email: diego.pena@usc.es

Leo Gross − *IBM Research Europe − Zurich, 8803 Rüschlikon, Switzerland;* orcid.org/0000-0002-5337-4159; Email: LGR@zurich.ibm.com

Authors

Valentina Malave − *Center for Research in Biological Chemistry and Molecular Materials, and Department of Organic Chemistry, University of Santiago de Compostela, 15782 Santiago de Compostela, Spain*

Rasmus Svensson − *Department of Physics and Competence Centre for Catalysis, Chalmers University of Technology, 412 96 Göteborg, Sweden*

Henrik Grönbeck − *Department of Physics and Competence Centre for Catalysis, Chalmers University of Technology, 412 96 Göteborg, Sweden*

Florian Albrecht − *IBM Research Europe − Zurich, 8803 Rüschlikon, Switzerland;* orcid.org/0000-0002-7418-9155

Complete contact information is available at: https://pubs.acs.org/10.1021/jacs.5c16196

Author Contributions

#V.M. and R.S. contributed equally.

Notes

The authors declare no competing financial interest.

■ ACKNOWLEDGMENTS

The authors thank Katja-Sophia Csizi and Lisanne Sellies for discussions. This study has received funding from the European Research Council Synergy grant MolDAM (grant number 951519), the Spanish Agencia Estatal de Investigación (grant number PID2022-140845OB-C62), Xunta de Galicia (Centro de Investigación do Sistema Universitario de Galicia, 2023−2027, grant number ED431G 2023/03), the European Regional Development Fund, and the Swedish Research Council (grant number 2024-05250). The calculations were performed at PDC and NSC via a grant from the National Academic Infrastructure for Supercomputing in Sweden (NAISS).

■ REFERENCES

(1) Jurczyk, J.; Woo, J.; Kim, S. F.; Dherange, B. D.; Sarpong, R.; Levin, M. D. Single-Atom Logic for Heterocycle Editing. *Nat. Synth* **2022**, *1* (5), 352−364.

(2) Campos, K. R.; Coleman, P. J.; Alvarez, J. C.; Dreher, S. D.; Garbaccio, R. M.; Terrett, N. K.; Tillyer, R. D.; Truppo, M. D.; Parmee, E. R. The Importance of Synthetic Chemistry in the Pharmaceutical Industry. *Science* **2019**, *363* (6424), No. eaat0805.

(3) Li, E.-Q.; Lindsley, C. W.; Chang, J.; Yu, B. Molecular Skeleton Editing for New Drug Discovery. *J. Med. Chem.* **2024**, *67* (16), 13509−13511.

(4) Ditzler, R. A. J.; Zhukhovitskiy, A. V. Sigmatropic Rearrangements of Polymer Backbones: Vinyl Polymers from Polyesters in One Step. *J. Am. Chem. Soc.* **2021**, *143* (48), 20326−20331.

(5) Kennedy, S. H.; Dherange, B. D.; Berger, K. J.; Levin, M. D. Skeletal Editing through Direct Nitrogen Deletion of Secondary Amines. *Nature* **2021**, *593* (7858), 223−227.

(6) Bartholomew, G. L.; Carpaneto, F.; Sarpong, R. Skeletal Editing of Pyrimidines to Pyrazoles by Formal Carbon Deletion. *J. Am. Chem. Soc.* **2022**, *144* (48), 22309−22315.

(7) Chen, L.-Y.; Li, J. Skeletal Editing of Dibenzolactones to Fluorenes via Ni- or Pd-Catalyzed Decarboxylation. *J. Org. Chem.* **2023**, *88* (14), 10252−10256.

(8) Dherange, B. D.; Kelly, P. Q.; Liles, J. P.; Sigman, M. S.; Levin, M. D. Carbon Atom Insertion into Pyrroles and Indoles Promoted by Chlorodiazirines. *J. Am. Chem. Soc.* **2021**, *143* (30), 11337−11344.
(9) Reisenbauer, J. C.; Green, O.; Franchino, A.; Finkelstein, P.; Morandi, B. Late-Stage Diversification of Indole Skeletons through Nitrogen Atom Insertion. *Science* **2022**, *377* (6610), 1104−1109.
(10) Finkelstein, P.; Reisenbauer, J. C.; Botlik, B. B.; Green, O.; Florin, A.; Morandi, B. Nitrogen Atom Insertion into Indenes to Access Isoquinolines. *Chem. Sci.* **2023**, *14* (11), 2954−2959.
(11) Luu, Q. H.; Li, J. A C-to-O Atom-Swapping Reaction Sequence Enabled by Ni-Catalyzed Decarbonylation of Lactones. *Chem. Sci.* **2022**, *13* (4), 1095−1100.
(12) Patel, S. C.; Burns, N. Z. Conversion of Aryl Azides to Aminopyridines. *J. Am. Chem. Soc.* **2022**, *144* (39), 17797−17802.
(13) Zhong, H.; Egger, D. T.; Gasser, V. C. M.; Finkelstein, P.; Keim, L.; Seidel, M. Z.; Trapp, N.; Morandi, B. Skeletal Metalation of Lactams through a Carbonyl-to-Nickel-Exchange Logic. *Nat. Commun.* **2023**, *14* (1), 5273.
(14) Jurczyk, J.; Lux, M. C.; Adpressa, D.; Kim, S. F.; Lam, Y.; Yeung, C. S.; Sarpong, R. Photomediated Ring Contraction of Saturated Heterocycles. *Science* **2021**, *373* (6558), 1004−1012.
(15) Kelley, B. T.; Walters, J. C.; Wengryniuk, S. E. Access to Diverse Oxygen Heterocycles via Oxidative Rearrangement of Benzylic Tertiary Alcohols. *Org. Lett.* **2016**, *18* (8), 1896−1899.
(16) Pavliček, N.; Gross, L. Generation, Manipulation and Characterization of Molecules by Atomic Force Microscopy. *Nat. Rev. Chem.* **2017**, *1* (1), No. 0005.
(17) Phark, S.; Weber, B.; Yoshida, Y.; Forrester, P. R.; Elbertse, R. J. G.; Stroscio, J. A.; Wang, H.; Yang, K.; Gross, L.; Mishra, S.; Paschke, F.; Kaiser, K.; Fatayer, S.; Repp, J.; Anderson, H.; Peña, D.; Albrecht, F.; Giessibl, F. J.; Fasel, R.; Fernández-Rossier, J.; Kawai, S.; Limot, L.; Lorente, N.; Jaeck, B.; Huang, H.; Ankerhold, J.; Ast, C. R.; Trahms, M.; Winkelmann, C.; Franke, K. J.; Soldini, M.; Wagner, G.; Neupert, T.; Küster, F.; Das, S.; Parkin, S.; Sessi, P.; Wang, Z.; Madhavan, V.; Huber, R.; Singh, G.; Donati, F.; Rusponi, S.; Brune, H.; Moreno-Pineda, E.; Ruben, M.; Wernsdorfer, W.; Huang, W.; Au-Yeung, K. H.; Willke, P.; Heinrich, A. J.; Baumann, S.; Loth, S.; Veldman, L. M.; Otte, S.; Wolf, C.; Sellies, L.; Schofield, S. R.; Flatte, M. E.; Keizer, J. G.; Simmons, M. Y. Roadmap on Atomically-Engineered Quantum Platforms. *Nano Futures* **2025**, *9*, 032001.
(18) Albrecht, F.; Fatayer, S.; Pozo, I.; Tavernelli, I.; Repp, J.; Peña, D.; Gross, L. Selectivity in Single-Molecule Reactions by Tip-Induced Redox Chemistry. *Science* **2022**, *377* (6603), 298−301.
(19) Albrecht, F.; Rončević, I.; Gao, Y.; Paschke, F.; Baiardi, A.; Tavernelli, I.; Mishra, S.; Anderson, H. L.; Gross, L. The Odd-Number Cyclo[13]Carbon and Its Dimer, Cyclo[26]Carbon. *Science* **2024**, *384* (6696), 677−682.
(20) Schuler, B.; Fatayer, S.; Mohn, F.; Moll, N.; Pavliček, N.; Meyer, G.; Peña, D.; Gross, L. Reversible Bergman Cyclization by Atomic Manipulation. *Nat. Chem.* **2016**, *8* (3), 220−224.
(21) Kawai, S.; Sang, H.; Kantorovich, L.; Takahashi, K.; Nozaki, K.; Ito, S. An Endergonic Synthesis of Single Sondheimer-Wong Diyne by Local Probe Chemistry. *Angew. Chem., Int. Ed.* **2020**, *59* (27), 10842−10847.
(22) Pavliček, N.; Schuler, B.; Collazos, S.; Moll, N.; Pérez, D.; Guitián, E.; Meyer, G.; Peña, D.; Gross, L. On-Surface Generation and Imaging of Arynes by Atomic Force Microscopy. *Nat. Chem.* **2015**, *7* (8), 623−628.
(23) Urgel, J. I.; Hayashi, H.; Di Giovannantonio, M.; Pignedoli, C. A.; Mishra, S.; Deniz, O.; Yamashita, M.; Dienel, T.; Ruffieux, P.; Yamada, H.; Fasel, R. On-Surface Synthesis of Heptacene Organometallic Complexes. *J. Am. Chem. Soc.* **2017**, *139* (34), 11658−11661.
(24) Eimre, K.; Urgel, J. I.; Hayashi, H.; Di Giovannantonio, M.; Ruffieux, P.; Sato, S.; Otomo, S.; Chan, Y. S.; Aratani, N.; Passerone, D.; Gröning, O.; Yamada, H.; Fasel, R.; Pignedoli, C. A. On-Surface Synthesis and Characterization of Nitrogen-Substituted Undecacenes. *Nat. Commun.* **2022**, *13* (1), 511.
(25) Pavliček, N.; Mistry, A.; Majzik, Z.; Moll, N.; Meyer, G.; Fox, D. J.; Gross, L. Synthesis and Characterization of Triangulene. *Nat. Nanotechnol.* **2017**, *12* (4), 308−311.
(26) Mishra, S.; Vilas-Varela, M.; Lieske, L.-A.; Ortiz, R.; Fatayer, S.; Rončević, I.; Albrecht, F.; Frederiksen, T.; Peña, D.; Gross, L. Bistability between π-Diradical Open-Shell and Closed-Shell States in Indeno[1,2-*a*]Fluorene. *Nat. Chem.* **2024**, *16* (5), 755−761.
(27) Schulz, F.; García, F.; Kaiser, K.; Pérez, D.; Guitián, E.; Gross, L.; Peña, D. Exploring a Route to Cyclic Acenes by On-Surface Synthesis. *Angew. Chem., Int. Ed.* **2019**, *58* (27), 9038−9042.
(28) Majzik, Z.; Cuenca, A. B.; Pavliček, N.; Miralles, N.; Meyer, G.; Gross, L.; Fernández, E. Synthesis of a Naphthodiazaborinine and Its Verification by Planarization with Atomic Force Microscopy. *ACS Nano* **2016**, *10* (5), 5340−5345.
(29) Lieske, L.-A.; Oechsle, A. H.; Rončević, I.; Gazizullin, I.; Albrecht, F.; Krinninger, M.; Grill, L.; Esch, F.; Gross, L. Tip-Induced Nitrene Generation. *ACS Nano* **2025**, *19* (35), 31572−31581.
(30) Kawai, S.; Krejčí, O.; Nishiuchi, T.; Sahara, K.; Kodama, T.; Pawlak, R.; Meyer, E.; Kubo, T.; Foster, A. S. Three-Dimensional Graphene Nanoribbons as a Framework for Molecular Assembly and Local Probe Chemistry. *Sci. Adv.* **2020**, *6* (9), No. eaay8913.
(31) Pavliček, N.; Gawel, P.; Kohn, D. R.; Majzik, Z.; Xiong, Y.; Meyer, G.; Anderson, H. L.; Gross, L. Polyyne Formation via Skeletal Rearrangement Induced by Atomic Manipulation. *Nat. Chem.* **2018**, *10* (8), 853−858.
(32) Kawai, S.; Silveira, O. J.; Kurki, L.; Yuan, Z.; Nishiuchi, T.; Kodama, T.; Sun, K.; Custance, O.; Lado, J. L.; Kubo, T.; Foster, A. S. Local Probe-Induced Structural Isomerization in a One-Dimensional Molecular Array. *Nat. Commun.* **2023**, *14* (1), 7741.
(33) Cai, J.; Pignedoli, C. A.; Talirz, L.; Ruffieux, P.; Söde, H.; Liang, L.; Meunier, V.; Berger, R.; Li, R.; Feng, X.; Müllen, K.; Fasel, R. Graphene Nanoribbon Heterojunctions. *Nat. Nanotechnol.* **2014**, *9* (11), 896−900.
(34) Nguyen, G. D.; Tsai, H.-Z.; Omrani, A. A.; Marangoni, T.; Wu, M.; Rizzo, D. J.; Rodgers, G. F.; Cloke, R. R.; Durr, R. A.; Sakai, Y.; Liou, F.; Aikawa, A. S.; Chelikowsky, J. R.; Louie, S. G.; Fischer, F. R.; Crommie, M. F. Atomically Precise Graphene Nanoribbon Heterojunctions from a Single Molecular Precursor. *Nat. Nanotechnol.* **2017**, *12* (11), 1077−1082.
(35) Gröning, O.; Wang, S.; Yao, X.; Pignedoli, C. A.; Borin Barin, G.; Daniels, C.; Cupo, A.; Meunier, V.; Feng, X.; Narita, A.; Müllen, K.; Ruffieux, P.; Fasel, R. Engineering of Robust Topological Quantum Phases in Graphene Nanoribbons. *Nature* **2018**, *560* (7717), 209−213.
(36) Rizzo, D. J.; Veber, G.; Cao, T.; Bronner, C.; Chen, T.; Zhao, F.; Rodriguez, H.; Louie, S. G.; Crommie, M. F.; Fischer, F. R. Topological Band Engineering of Graphene Nanoribbons. *Nature* **2018**, *560* (7717), 204−208.
(37) Friedrich, N.; Brandimarte, P.; Li, J.; Saito, S.; Yamaguchi, S.; Pozo, I.; Peña, D.; Frederiksen, T.; Garcia-Lekue, A.; Sánchez-Portal, D.; Pascual, J. I. Magnetism of Topological Boundary States Induced by Boron Substitution in Graphene Nanoribbons. *Phys. Rev. Lett.* **2020**, *125* (14), No. 146801.

https://doi.org/10.1021/jacs.5c16196
J. Am. Chem. Soc. 2025, 147, 44055−44059